Large-Scale Parallel Uncontracted Multireference-Averaged Quadratic Coupled Cluster: The Ground State of the Chromium Dimer Revisited†

Thomas Müller*

Institute of Advanced Simulation, Jülich Supercomputing Center, Research Centre Jülich, D-52425 Jülich, Germany

Received: June 4, 2009; Revised Manuscript Received: July 29, 2009

The accurate prediction of the potential energy function of the $X^1\Sigma_g^+$ state of Cr_2 is a remarkable challenge; large differential electron correlation effects, significant scalar relativistic contributions, the need for large flexible basis sets containing g functions, the importance of semicore valence electron correlation, and its multireference nature pose considerable obstacles. So far, the only reasonable successful approaches were based on multireference perturbation theory (MRPT). Recently, there was some controversy in the literature about the role of error compensation and systematic defects of various MRPT implementations that cannot be easily overcome. A detailed basis set study of the potential energy function is presented, adopting a variational method. The method of choice for this electron-rich target with up to 28 correlated electrons is fully uncontracted multireference-averaged quadratic coupled cluster (MR-AQCC), which shares the flexibility of the multireference configuration interaction (MRCI) approach and is, in addition, approximately size-extensive (0.02 eV in error as compared to the MRCI value of 1.37 eV for two noninteracting chromium atoms). The best estimate for D_e arrives at 1.48 eV and agrees well with the experimental data of 1.47 ± 0.056 eV. At the estimated CBS limit, the equilibrium bond distance (1.685 Å) and vibrational frequency (459 cm^{-1}) are in agreement with experiment (1.679 Å, 481 cm^{-1}). Large basis sets and reference configuration spaces invariably result in huge wave function expansions (here, up to 2.8 billion configuration state functions), and efficient parallel implementations of the method are crucial. Hence, relevant details on implementation and general performance of the parallel program code are discussed as well.

1. Introduction

The chromium dimer is a notoriously difficult target for ab initio methods in quantum chemistry, with a long history of attempts to tackle the problem. Its $X^1\Sigma_g^+$ ground state formally contains a hextuple bond with six bonding orbitals ($3d_\sigma$, $3d_\pi$, $3d_{\pi'}$, $3d_\delta$, $3d_{\delta'}$, $4s_\sigma$) derived from the 3d and 4s atomic orbitals. The molecule dissociates into two chromium atoms in their high-spin ground state (^7S). The ground state of the chromium dimer has been experimentally characterized by measurements of the A ← X transition.[1] A vibrational frequency ω_e of 452 cm^{-1} and a short bond length of 1.679 Å, agreeing with the high formal bond order, have been assigned. In contrast, the experimental binding energy[2] of 1.44 ± 0.05 eV is even less than the 2.078 eV determined for singly bonded Cu.[3] For the isovalent Mo_2 analogue, relativistic effects stabilize the ground state to 4.41 eV. The effective bond order[4,5] (EBO), a simple measure of the bond applicable to multiconfigurational wave functions, indicates that the Mo_2 EBO value[6] of 5.2 comes much closer to the limiting value of 6 than Cr_2 with an EBO of 4.5, both derived from complete active space peturbation theory second order (CASPT2).[7,8] An accurate experimental potential energy function based on photoelectron spectrosopy on Cr_2^- sparked new interest in this molecule.[9] The potential curve shows an unusual shape with a broad "shelf" on the outer wall. While the inner well is dominated by 3d−3d bonding, the broad shelf corresponds to predominantly 4s−4s bonding with antiferromagnetically coupled 3d electrons. A very shallow minimum in the 4s−4s bonding region could not be confirmed unambiguously on experimental grounds.[9]

The $X^1\Sigma_g^+$ state of Cr_2 is characterized by large differential electron correlation effects. The description of bond polarization at short distances requires at least f functions, and semicore valence electron correlation must not be neglected. The accurate calculation of the spectroscopic constants and the potential energy function for Cr_2 constitutes a prominent demanding benchmark test case for electron correlation methods.

The multiconfigurational character and the near-degeneracies of low-lying electronic states is characteristic for many open-shell transition-metal compounds. Dynamical electron correlation effects are as large as scalar relativistic corrections. Not unexpectedly, single-reference electron correlation methods do not perform well here; starting from a symmetry-broken unrestricted Hartree−Fock wave function, unrestricted coupled cluster singles and doubles with perturbative triples correction predicted a dissociation energy of 0.89 eV and a bond distance of 2.54 Å.[10] Density functional theory calculations[10−20] have not been particularly successful either, owing to the large spread of the results depending upon the specific functional used. Spurious spin contamination adds to the uncertainties of unrestricted treatments.

Multireference methods face computational difficulties arising from the large reference configuration space; even the smallest possible complete active space (CAS) with 12 electrons in the 12 valence orbitals, which dissociates correctly, consists of 28784 configurations in D_{2h} symmetry, and extension by four 4p-derived orbitals gives already rise to ∼1.8 million configurations. At the complete active space self-consistent field (CASS-

† Part of the "Russell M. Pitzer Festschrift".

* E-mail th.mueller@fz-juelich.de.

10.1021/jp905254u CCC: $40.75
Published on Web 09/02/2009

CF)[21] level of theory, the ground state is very weakly bound in the 4s−4s bonding region using a CAS(12,12),[22] while adding a subset of four 4p-derived orbitals into the active space to yield CAS(12,16) causes this minimum becomes more pronounced.[23] Thus, in order to account for dynamic electron correlation, computationally less demanding MRPT methods were the preferred tool to investigate this molecule, despite restrictions on the size of the active space. Early applications disagreed with the experimental data. Finally, CASPT2 calculations[23] conducted with large basis sets including g functions, semicore 3s and 3p electron correlation, and scalar relativistic effects in all-electron calculations led to satisfactory agreement with the experimental data, and the problem was considered to be settled.

More recently, a detailed analysis of MRPT and MRCI results obtained with basis sets including up to i functions,[24] however, revealed that MRPT methods give rise to a systematic error that was traced back to an imbalanced treatment of core−valence and valence−valence electron correlation. It was argued that the excellent results obtained in ref 23 are due to fortituous error compensation. This shortcoming is shared by several implementations of MRPT second order, which are either free (*N*-electron valence state perturbation theory (NEVPT2))[25−28] or less plagued by intruder states (CIPT2, which treats valence and core electron correlation at MRCI and PT2 levels, respectively)[24] than CASPT2, so that level-shift techniques[29,30] (required to overcome the intruder state instabilities) cannot be responsible for this defect. Close to the complete basis set (CBS) limit, CASPT2 and NEVPT2 overbind by up to 0.4 eV, while CIPT2 underestimates D_e by 0.3 eV. CASPT2-based r_e agrees with the experimental bond length, while NEVPT2 is short by 0.02 Å, and CIPT2 exceeds by 0.08 Å. Perturbation theory third order (NEVPT3) produces disappointing results,[31] which is likely due to the sensitivity to the choice of the zeroth-order approximation $\hat{H}_0$. It is well-known that perturbation theory second order benefits from error compensation effects, and including higher-order corrections magnifies shortcomings in $\hat{H}_0$ which are otherwise not apparent at second order. While Celani et al.[24] succeeded in obtaining satisfactory equilibrium bond length and vibrational harmonic frequencies with internally contracted (IC) MR-CI[32] with and without a posteriori size-extensivity corrections of Davidson type,[33] D_e was underestimated by 0.5 and 0.7 eV even for extended basis sets. For an overview over previous calculations, refer to Figure 5 and Table 2, respectively, in the Results and Discussion section.

The purpose of this work is to resolve the apparent contradictions with respect to MRPT approaches by accurately computing the potential energy function of the $X^1\Sigma_g^+$ state by a different multireference method, under special consideration of the bottlenecks identified by previous workers. The method of choice is MR-AQCC,[34,35] an approximately size-extensive functional closely related to MRCI, which is expected to be more adequate for this problem than MRCI with a posteriori Davidson correction or MRPT. To eliminate the differential internal contraction error, estimated to contribute as much as 0.09 eV to D_e for valence electron correlation,[24] fully uncontracted MR-AQCC is employed. Scalar relativistic effects are taken into account by the Douglas−Kroll−Hess (DKH) Hamiltonian[36,37] as to avoid the uncertainties arising from atom-optimized effective core potentials. This is complemented by a study of basis set dependence and extrapolation to the CBS limit.

Uncontracted MR-AQCC calculations with large basis sets invariably encounter huge CI expansions, and efficient parallel implementations are of crucial importance. While the general parallelization scheme based on a partitioning of the CI vector into segments and computing the individual partial contributions (tasks) independently in a single loop over all tasks is fairly straightforward,[38] load balancing issues become critical as the optimum task definition depends on both machine- (e.g., bandwidth, memory per node, clock rate, number of nodes, etc.) and model-specific parameters (basis set, point group symmetry, configuration space). With the increasing availability of large-scale supercomputer systems (nowadays, mostly large clusters of multiway shared memory systems) with up to several thousands of processors, it is yet not straightforward to make use of the inherent computational power of these systems. Hence, conceptual and performance issues relevant for large-scale applications are also discussed.

2. Methodology

This section briefly describes aspects and modifications of the MR-CISD method as implemented in the COLUMBUS program system[39−42] that are relevant to its usage on massive-parallel computer systems for large-scale calculations. These considerations also apply to the approximately size-extensive methods MR-ACPF (averaged coupled pair functional),[43] MR-AQCC (averaged quadratic coupled cluster),[34,35] LRT (linear response theory)-MR-AQCC,[44] and TE(total energy)-MR-AQCC,[45] which are closely related to MR-CISD.

The many-electron wave function is expanded in terms of spin-adapted configuration state functions (CSFs) Φ_i. The full CI space is partitioned into four disjoint subspaces P, Q′, Q, and R. P denotes the reference configuration space, spanned by a subset of all configurations that can be obtained by distributing the electrons over the internal (active + inactive) orbitals, only. Q′ denotes all single and double excitations out of $\Phi_i \in$ P not contained in P with all external orbitals unoccupied (also termed internal configurations), while Q contains those single and double excitations not contained in either P or Q′. R finally denotes all CSFs not contained in either P, Q, or Q′.

The full CI wave function reads

$$\Psi^{\mathrm{FCI}} = \Psi_{\mathrm{P}} + \Psi_{\mathrm{Q}'} + \Psi_{\mathrm{Q}} + \Psi_{\mathrm{R}} = \sum_{i\in \mathrm{P}} c_i^{\mathrm{P}}\Phi_i^{\mathrm{P}} + \sum_{i\in \mathrm{Q}'} c_i^{\mathrm{Q}'}\Phi_i^{\mathrm{Q}'} + \sum_{i\in \mathrm{Q}} c_i^{\mathrm{Q}}\Phi_i^{\mathrm{Q}} + \sum_{i\in \mathrm{R}} c_i^{\mathrm{R}}\Phi_i^{\mathrm{R}} \quad (1)$$

The uncontracted MR-CISD expansion is truncated to $\Psi_{\mathrm{P}} + \Psi_{\mathrm{Q}'} + \Psi_{\mathrm{Q}}$, with all $c_i^{\mathrm{P}}, c_i^{\mathrm{Q}'}, c_i^{\mathrm{Q}}$ optimized independently. As the truncated MR-CISD expansion is not size-extensive, a rapidly increasing differential electron correlation error is introduced beyond about 10 correlated electrons. Approximately, size-extensivity corrected methods restore size-extensivity by incorporating the effect of higher excitations from the R space in an approximate way. MR-AQCC includes the effect of disconnected quadruple excitations and may be considered as an approximation to MR-CCSD. As a variational method with respect to the wave function expansion coefficients, analytical gradients can be implemented efficiently, exploiting the Hellmann−Feynman theorem.[46] Very accurate data for excitation energies, equilibrium bond lengths, and harmonic frequencies have been obtained at the CBS limit in a benchmark study.[47] Thus, it is the method of choice for many-electron targets.

MR-CISD, MR-AQCC, and MR-ACPF can be expressed in terms of optimizing the following functional of the correlation energy with respect to the wave function expansion coefficients c_i^{α} of state α

$$F_\alpha(\mathbf{c}^\alpha) = \frac{\langle \sum_i c_i^\alpha \Phi_i | \hat{H} - E_0^\alpha | \sum_i c_i^\alpha \Phi_i \rangle}{\sum_{i\in \mathrm{P,Q'}} (c_i^\alpha)^2 + G \sum_{i\in \mathrm{Q}} (c_i^\alpha)^2} \tag{2}$$

where the constant G equals 1 for MRCISD, $2/n_e$ for MRACPF, and $1 - \{[(n_e - 3)(n_e - 2)]/[n_e(n_e - 1)]\}$ for MRAQCC, with n_e being the number of correlated electrons, only. The reference energy E_0^α of the reference wave function is independent of c_i^α. Equivalently, this method may be formulated in terms of an eigenvalue problem with a diagonal shift of the Q space CSFs.

$$\langle \Phi_j | \hat{H} - E_0^\alpha + \hat{\Delta}_\alpha | \sum_i c_i^\alpha \Phi_i \rangle = \Delta E_\alpha c_j^\alpha \tag{3}$$

$$\hat{\Delta}_\alpha = \sum_{k\in \mathrm{Q}} (1 - G) \Delta E_\alpha |\Phi_k\rangle\langle\Phi_k| \tag{4}$$

As $\hat{\Delta}_\alpha$ depends on the state-specific correlation energy $\Delta E_\alpha = E - E_0^\alpha$, the equations have to be solved iteratively with ΔE_α approximated by the current correlation energy estimate. Most conveniently, the subspace representation $\hat{\Delta}_\alpha$ is added to the subspace Hamiltonian. Densities are obtained through scaling of the CI-like density ${}^{\mathrm{CI}}\Gamma^\alpha$ and reference density matrix elements $\Gamma_{\mathrm{P}}^\alpha$.

$$\Gamma^\alpha = a\,{}^{\mathrm{CI}}\Gamma^\alpha + (1 - a)\Gamma_{\mathrm{P}}^\alpha \tag{5}$$

$$a = \frac{\sum_i (c_i)^2}{\sum_{i\in \mathrm{P,Q'}} (c_i)^2 + G \sum_{i\in \mathrm{Q}} (c_i)^2} \tag{6}$$

In contrast to state-specific energies and properties, transition densities are not accessible. Linear response theory (LRT) derives excited states perturbatively from the reference state, usually the ground state. The LRT variant of MR-AQCC allows for the consistent calculation of excitation energies and transition densities at the expense of the LRT approximation. The formulas resemble those above, substituting the state-specific correlation energy ΔE_α with the correlation energy of the reference state and the density matrices with the corresponding transition densities between the reference and excited-state α throughout. MR-AQCC/MR-ACPF implicitly assume a qualitatively correct reference wave function through E_0^α, which enters $\hat{\Delta}_\alpha$, a requirement that can rarely be met for strongly interacting electronic states close to avoided crossings. The total energy (TE) variant of MR-AQCC replaces $F_\alpha(\mathbf{c}^\alpha)$ by a functional of the total energy, and E_0^α is substituted by the relaxed reference energy $\tilde{E}_0^\alpha$ defined as

$$\tilde{E}_0^\alpha = \frac{\langle \sum_{i\in \mathrm{P}} c_i^\alpha \Phi_i^\alpha | \hat{H} | \sum_{i\in \mathrm{P}} c_i^\alpha \Phi_i^\alpha \rangle}{\sum_{i\in \mathrm{P}} (c_i^\alpha)^2} \geq E_0^\alpha \tag{7}$$

It follows that $\hat{\Delta}$ is amended by an off-diagonal term $\hat{\tilde{\Delta}}$ over the reference space, only.

$$\hat{\tilde{\Delta}} = \sum_{l\in \mathrm{P}} \sum_{k\in \mathrm{P}} \left(|\Phi_l\rangle\langle\Phi_l| \frac{(G - 1) \sum_{i\in \mathrm{Q}} (c_i^\alpha)^2}{\sum_{i\in \mathrm{P}} (c_i^\alpha)^2} (\hat{H} - \tilde{E}_0^\alpha) |\Phi_k\rangle\langle\Phi_k| \right) \tag{8}$$

TE-AQCC is sensitive to the choice of the reference space, only, similar to the multireference analogues of the SDCI type Davidson correction[46]

$$E^{\mathrm{CI+Q1}} = E_{\mathrm{CI}}^\alpha + (E_{\mathrm{CI}}^\alpha - \tilde{E}_0^\alpha)(1 - c_0^2) \tag{9}$$

$$E^{\mathrm{CI+Q2}} = E_{\mathrm{CI}}^\alpha + (E_{\mathrm{CI}}^\alpha - \tilde{E}_0^\alpha)\frac{1 - c_0^2}{c_0^2} \tag{10}$$

$$E^{\mathrm{CI+Q3}} = E_{\mathrm{CI}}^\alpha + (E_{\mathrm{CI}}^\alpha - \tilde{E}_0^\alpha)\frac{1 - c_0^2}{2c_0^2 - 1} \tag{11}$$

where $c_0^2 = \sum_{i\in \mathrm{P}} c_i^\alpha \Phi_i^\alpha$ denotes the relaxed weight of the reference space in the final normalized MR-CISD wave function.

The size-extensivity correction for MR-AQCC and MR-ACPF takes the form of a shift of the diagonal **H** matrix elements belonging to the Q space. This may give rise to divergence of the energy. Assume a model CSF space solely consisting of a single Q and P configuration with the diagonal **H** matrix elements H_{Q} and H_{P}. The eigenvalues of the modified **H** matrix are to be computed self-consistently for Δ_α and E

$$\begin{pmatrix} \bar{H} + \delta + \Delta_\alpha & \alpha \\ \alpha & \bar{H} - \delta \end{pmatrix} \quad \begin{aligned} \bar{H} &= \frac{1}{2}(H_{\mathrm{Q}} + H_{\mathrm{P}}) \\ \delta &= \frac{1}{2}(H_{\mathrm{Q}} - H_{\mathrm{P}}) \geq 0 \\ \Delta_\alpha &= (1 - G)(E - H_{\mathrm{P}}) \leq 0 \end{aligned} \tag{12}$$

For the first cycle, Δ_α is set to 0, and the lowest eigenvalue E is given by

$$E = \bar{H} - \sqrt{\alpha^2 + \delta^2} \tag{13}$$

$$= \bar{H} - \delta - \frac{1}{2\delta}\alpha^2 + \mathcal{O}(\alpha^4) \tag{14}$$

$$\Delta_\alpha = -\frac{1}{2}(1 - G)\frac{\alpha^2}{\delta} \tag{15}$$

If $|\Delta_\alpha| < 2\delta$, divergence of the energy cannot be avoided. Divergence can occur whenever Δ_α is not converging to a finite asymptotic value. Expanding E up to third order in α around $\alpha = 0$ and reinserting it into the original eigenvalue problem shows that the expression for Δ_α remains unchanged in the subsequent iterations, and convergence is guaranteed if the ratio of α/δ is small enough for the fourth-order term of the Taylor expansion to vanish. The general case is divergent whenever $\Delta_\alpha + H_i < H_j \; \forall \; i \in \mathrm{Q}, j \in \mathrm{P,Q'}$, which again relies on the magnitude of the off-diagonal **H** matrix elements coupling to the Q space and the diagonal matrix element differences.

The evaluation of all functionals is based on the graphical unitary group approach.[48,49] Here, the wave function is specified

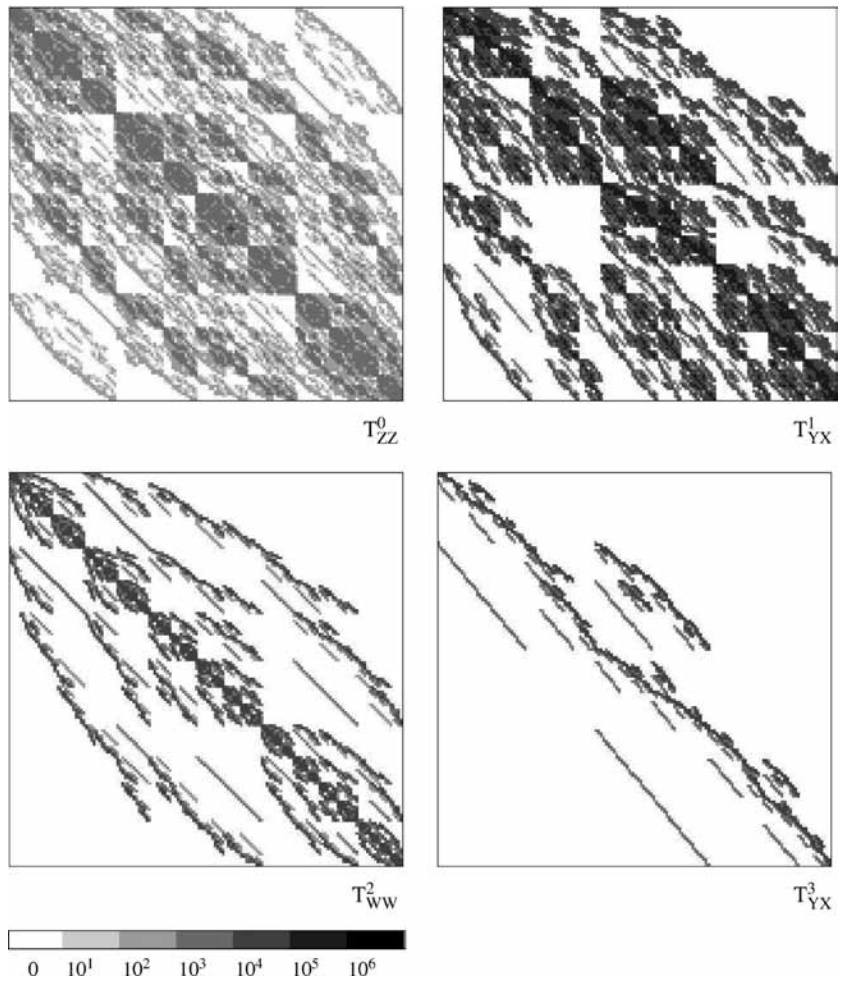

Figure 1. Cost matrix for a CAS(12,12) with all inactive electrons frozen (D_{2h}). The logarithmic gray scale of the patches encodes the relative work load required to compute the respective subblock of the CI matrix. The resolution is 150 × 150 blocks per task type $T^{I}_{ss'}$, corresponding to 192 Z, 2266 Y 1883 X, and 1132 W type encoded internal walks per block. For the EXTD basis with ∼35 orbitals per irrep, each block encodes 192 Z, 79 × 10^3 Y, 288 × 10^3 X, or 173 × 10^3 W configurations.

in terms of DRTs (distinct row tables), which are tabular representations of the distinct row graph with each CSF represented as a directed walk from tail to head. In the second-quantized form, the Hamiltonian can be written in terms of one- (h_{ij}) and two-electron MO integrals ($(ij|kl) = \langle i(1)j(1)|(1/\mathbf{r}_{12})|k(2)l(2)\rangle$) and the generators of the unitary group $U(n)$ ($\hat{E}_{ij}$)

$$\hat{H} = \sum_{ij} h_{ij}\hat{E}_{ij} + \frac{1}{2}\sum_{ijkl}(ij|kl)(\hat{E}_{ij}\hat{E}_{kl} - \delta_{jk}\hat{E}_{il}) \quad (16)$$

Evaluating the matrix element $\langle\Phi_m|\hat{H}|\Phi_n\rangle$ of the CI matrix $\mathbf{H}$ thus reduces to the computation of the respective coupling coefficients $\langle\Phi_m|\hat{E}_{ij}|\Phi_n\rangle$, $\langle\Phi_m|\hat{E}_{ij}i\hat{E}_{kl} - \delta_{jk}\hat{E}_{il}|\Phi_n\rangle$, and their contraction with the MO integrals. The GUGA formalism is used to efficiently evaluate the CI matrix elements on the fly, while the dimension of the CI vector retains the size of the encoded CSF space. A recently developed variant of GUGA-based CI[50] goes a step further and incorporates a nonlinearly contracted CI wave function expansion directly into the GUGA formalism, so that the number of variational parameters is several orders of magnitude smaller than the underlying encoded CSF basis. While the memory consumption compared to the traditional approach is negligible, the optimization of a huge number of linear parameters is replaced by a corresponding optimization of a much smaller set of nonlinear parameters.

3. Implementation

The orbital space is divided into n_{int} internal orbitals (indices i,j,k,l) occupied by at least one reference configuration and the remaining n_{ext} external orbitals (indices a,b,c,d) occupied by at most two electrons. The CSF space is partitioned into configurations containing no (Z), one (Y), two triplet (X), and two singlet (W) coupled electrons in the external orbital space, respectively. It is further segmented into continuously enumerated subsets, such that CSFs sharing the same internal orbital occupation and spin-coupling (denoted as internal walks) are collected into one segment. The integrals are classified according to the number of external orbital indices (0,1,2,3,4). The nonvanishing contributions $T^{\mathrm{I}}_{\mathrm{s,s'}}$ to the symmetric CI matrix are sketched in Figure 1. Each task type $T^{\mathrm{I}}_{\mathrm{s,s'}}$ is characterized by integral class I and the pair of segment types s,s′ (s,s′ ∈ Z,Y,X,W), while an individual task $T^{\mathrm{I}}_{\tilde{\mathrm{s}},\tilde{\mathrm{s}}'}$ carries the segment indices $\tilde{\mathrm{s}},\tilde{\mathrm{s}}'$. For four-external integrals, nonvanashing contributions arise only among CSFs sharing the same internal walk and, hence, occur solely within a single segment. With multiple segments per segment type, an almost arbitrary number of independent tasks can be generated and evaluated in any order. Spin−orbit CI introduces additional zero-, one-, and two-external one-electron spin−orbit integrals, and the associated terms are combined with the corresponding nonrelativistic task types. One-electron integral contributions not explicitly mentioned are combined with the most appropriate two-electron terms.

SCHEME 1: Schematic Picture of the Segmented Matrix Vector Multiple[a]

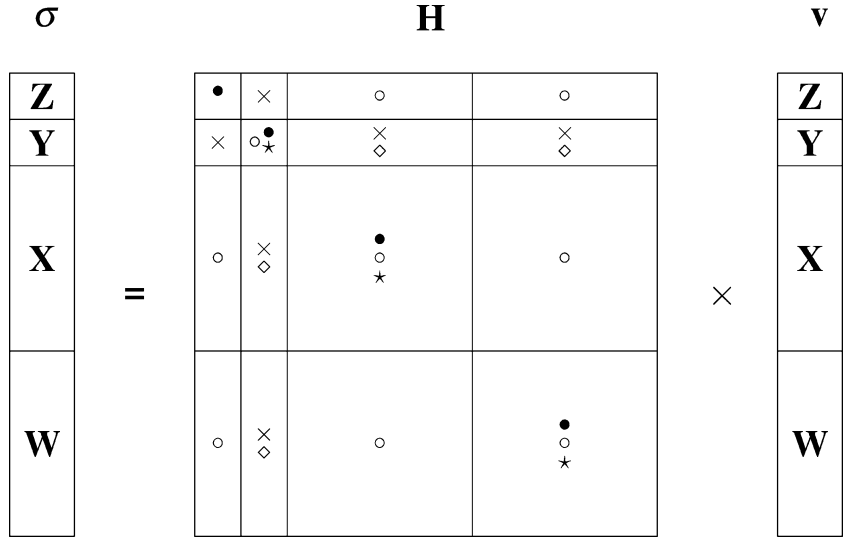

[a] Lines denote segment type boundaries (Z: all-internal; Y: one-external; X: triplet coupled two-external; and W: singlet coupled two-external CSFs), while symbols represent nonvanishing task types and integral classes, ●: $T^0_{ZZ},T^0_{YY},T^0_{XX},T^0_{WW}\{(ij|kl),h_{ij}\}$; ★: $T^4_Y,T^4_X,T^4_W\{(ab|cd),h_{ab}\}$; ×: $T^1_{YZ},T^1_{YW},T^1_{YX}\{(ij|ka)\}$; ○: $T^2_{YY},T^2_{XZ},T^2_{WZ},T^2_{WW},T^2_{XX},T^2_{WX}\{(ij|ab),(ia|jb)\}$; ◇: $T^3_{YW},T^3_{YX}\{(ia|bc),h_{ia}\}$; *i,j,k,l* and *a,b,c,d* denote internal and external orbital indices, respectively.

The direct CI approach[51] using the Davidson diagonalization[52,53] replaces the explicit construction of the CI matrix by an iteratively improved subspace representation of the problem. It relies on the efficient formation of matrix vector products $\sigma = \mathbf{Hv}$ (see Scheme 1). This procedure requires the storage of up to the predefined maximum of $n_{v\max}$ vectors $\mathbf{v}$ and σ, which constitute the basis of the subspace representation of $\mathbf{H}$. The evaluation of each partial contribution $T^I_{\tilde{s},\tilde{s}'}$ requires random access to a pair of σ_s and $\mathbf{v}_{s'}$ segments and a single pass through the integrals of class I. In order to minimize the bookkeeping overhead associated with coupling coefficient evaluation, segment-specific DRTs encoding solely the CSF subspace of a given segment are introduced. To further reduce overhead while retaining low local memory consumption tasks $T^I_{\tilde{s},\tilde{s}'}$ and $T^I_{\tilde{s}',\tilde{s}}$ are treated jointly at the expense of doubling the local memory consumption if $\tilde{s}',\tilde{s}$ contain at most a single unique X or W type segment. The major quantities to be stored and accessed are the $2n_{v\max}n_{csf}$ elements of the subspace basis vectors $(\mathbf{v}_i,\sigma_i)$ and the two-electron integrals $\sim n^{4-I}_{int}n^I_{ext}/8$. Subspace basis vectors and three- and four-external integrals contribute most to the storage requirements. Upon convergence of the energy, the one- and two-electron density matrices are evaluated using essentially the same machinery, with integrals replaced by density matrix elements at the expense of a single CI iteration.

In serial operation, the entire trial and σ vector are kept in memory while the integrals and subspace basis vectors are kept on disk with total storage requirements of $16n_{csf}$ bytes of memory and $16n_{csf}n_{v\max} + (n_{ext} + n_{int})^4$ bytes of disk space. The I/O intense step of forming and reducing the subspace representations of $\hat{H}$, $\hat{\Delta}$, and the overlap matrix employs the efficient linear COLUMBUS scheme described in ref 54. The entire density matrix is kept in memory to eliminate I/O overhead during the accumulation of the partial density matrix contributions.

In parallel mode, the subspace basis vectors are kept in distributed memory, such that all subspace manipulations operate on local data only. Integrals and density matrix elements are kept in memory throughout. The formation of the matrix−vector product and density matrices invariably involves interprocess communication to access nonlocal trial and σ vector segments and integrals. The preference for distributed and local memory merely reflects the I/O bottleneck on most (massive) parallel systems.

Partitioning the N_s CSFs of type s into n_s segments divides the total work of $T^I_{ss'}$ into $n_sn_{s'}$ tasks, each reading and writing one segment as well as running a single pass through all integrals of class I. The total data transfer volume $V^I_{ss'}$ (in Bytes) depends at most quadratically on the number of segments for the integral contribution and linearly on the σ and trial vector component

$$V^I_{ss'} = 8(n'_sN_s + n_sN'_s) + n_sn'_s(n_{int})^{4-I}(n_{ext})^I \qquad I < 4 \tag{17}$$

$$V^4_s = 16N_s + n_s(n_{ext})^4 \tag{18}$$

To feed n_{cpu} CPUs, ideally, it is sufficient to generate $\mathcal{O}(n_{cpu})$ tasks [i.e., $n_s = n'_s = \mathcal{O}(n_{cpu})^{1/2}$], so that the total communication volume scales $\mathcal{O}(n^\alpha_{cpu})$ with $1/2 \le \alpha \le 1$ and the average communication volume per CPU drops with increasing processor usage. The zero-, one-, and two-external integrals, which amount to only a small fraction of the total number of integrals, are, in practice, kept replicated on each CPU, so that the three-external integrals contribute formally quadratic to the communication volume. To this end, it is assumed that the workload is uniformly distributed among the tasks. Owing to the structure and sparsity of the CI matrix, this, however, is not the case. The total execution time $t^I_{\tilde{s}\tilde{s}'}$ for a task $T^I_{\tilde{s}\tilde{s}'}$ decomposes into

$$t^I_{\tilde{s}\tilde{s}'} = t_c + t_\sigma + t_d \approx \alpha n_c + \beta n_u + V^I_{\tilde{s}\tilde{s}'}/\gamma \qquad (I = 0,1,2,3) \tag{19}$$

$$t^4_{\tilde{s}} = t_\sigma + t_d \approx \beta' n_{CSF} + V^4_{\tilde{s}\tilde{s}'}/\gamma \tag{20}$$

(i) the data transfer time t_d, given by $V^I_{\tilde{s}\tilde{s}'}$ divided by some effective network bandwidth γ, (ii) the evaluation time t_d of

the internal contribution to the coupling coefficient, on average, proportional to their number of nonvanashing GUGA loops n_c, and (iii) the formation of the matrix vector product t_σ. The formation of the σ vector makes extensive use of linear algebra, and t_σ is, on average, proportional to the number of valid upper walks n_u, while the prefactor β depends on task type, point group symmetry, n_{ext}, and processor characteristics (e.g., cache, clock frequency). The t_σ can vary by many orders of magnitude even among tasks of the same type! Both n_u and n_c depend solely on the reference space definition, the number and ordering of internal orbitals, and the number of correlated electrons. Both quantities are entirely independent of the basis set size. The T^4_s tasks are special insofar as the computational cost is uniformly spread among all tasks and proportional to the length of the CI segment.

Figures 1 and 2 (referred to as a cost matrix) display n_u for a MR-AQCC calculation for the selected task types T^0_{ZZ}, T^1_{YX}, T^2_{WW}, and T^3_{YX} at a resolution of 150 × 150 segments (=22500 blocks). Since n_u and thus the cost matrix are independent of the basis set size, it is sensible to characterize each segment by the range of internal walks associated. The number of encoded CSFs for each segment is approximately obtained by scaling the number of internal walks with a factor of 1 (Z), n_{ext}/n_{irrep} (Y), and $n^2_{ext}/(2n_{irrep})$ (X,W), where n_{ext}/n_{irrep} denotes the average number of external orbitals per irreducible representation (irrep). The cost matrix for a CAS(12,12) with all inactive electrons frozen (Figure 1) is widely different from its counterpart for the direct product space chosen for Cr_2 with the 3p electrons correlated (Figure 2). The computational cost per segment block for any given task type can vary by up to 6 orders of magnitude. The discernible pattern of the cost matrix reflects the underlying permutational symmetry of the CSF space as exploited by the unitary group approach. The fraction of nonvanishing tasks decreases in the order $T^0_{s,s'}$, $T^1_{s,s'}$, $T^2_{s,s'}$, $T^3_{s,s'}$ from 65 to 7% (Figure 1) and 90 to 6% (Figure 2). The widely different cost matrices illustrate the difficulty to ensure load balancing without excessive data transfer load. In fact, it is tedious to guess or to iteratively improve the load balancing even for a modest number of CPUs (say 64) without a priori knowledge of the structural information provided by the cost matrix. Even with dynamic load balancing (implemented through a shared counter and a time-ordered task list), the specification of the number of segments and segment bounderies to prevent monopolizing a calculation by a few tasks while keeping communication overhead within bounds requires this information.

While for a small number of CPUs on a shared-memory machine (i.e., fast communication), it is straightforward to achieve load balancing, for the general case, it is no longer practical to set up the segmentation manually. Instead, an iterative numerical procedure has been devised to generate a list of nonvanishing tasks from the cost matrix and scaling factors constrained to minimum data transfer volume, optimum

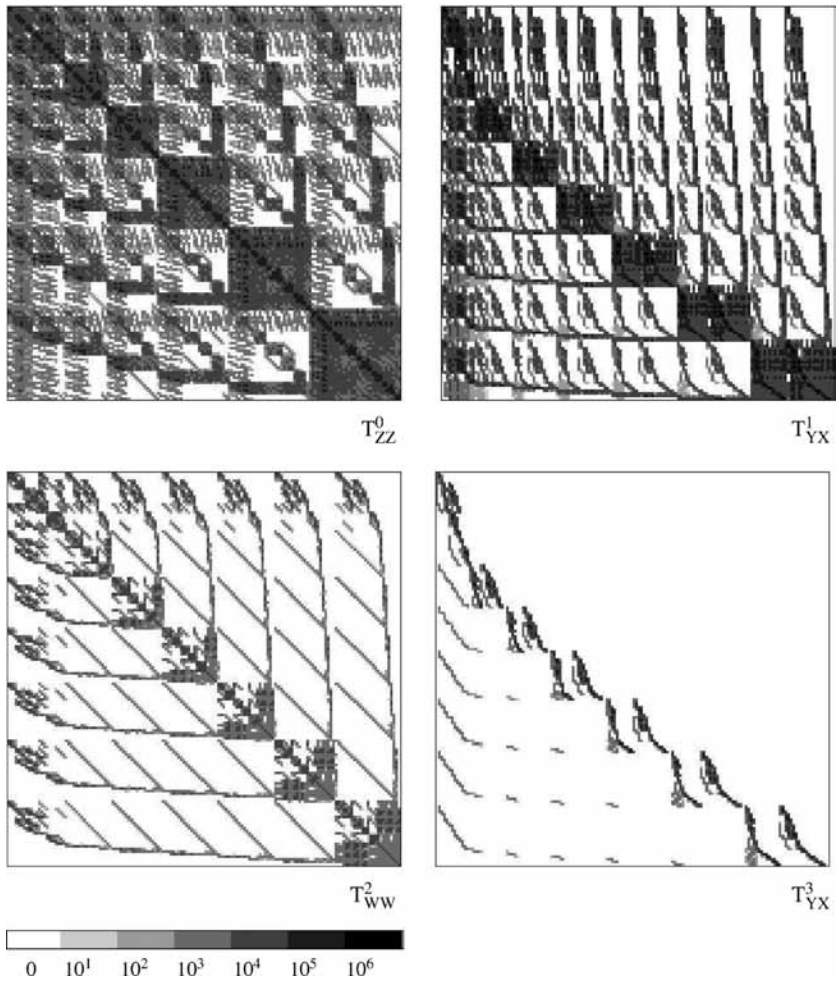

Figure 2. Cost matrix for a direct product space used for Cr_2 with 3p electrons correlated. The logarithmic gray scale of the patches encodes the relative work load required to compute the respective subblock of the CI matrix. The resolution is 150 × 150 blocks per task type $T^I_{ss'}$ corresponding to 1825 Z, 2266 Y 1883 X, and 1132 W type encoded internal walks per block. For the EXTD basis with ~35 orbitals per irrep, each segment encodes 1825 Z, 365 × 10^3 Y, 5500 × 10^3 X, or 5500 × 10^3 W configurations.

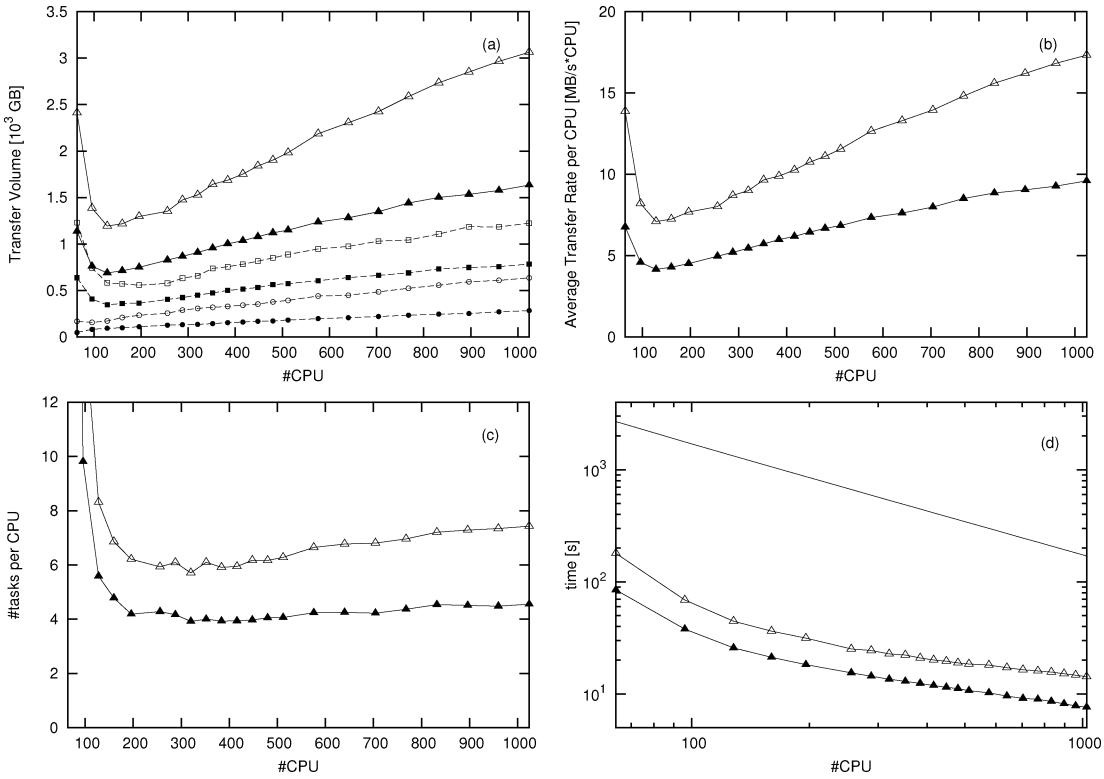

Figure 3. Performance behavior of the MR-AQCC code; (a) total data transfer volume, (b) average transfer rate per CPU, (c) average number of tasks per CPU, and (d) estimated communication time (solid line with symbols) and total wall clock time per CI iteration (solid line). Open and filled triangles denote dynamic and semistatic load balancing, respectively. Dashed lines indicate partial contributions of all tasks processing two external (squares) and three external integrals (circles).

load balancing, maximum memory usage, and number of CPUs. For a wide range of configuration spaces and molecules, it has been found that excellent load balancing and scalability can be achieved. Such a scheme relies on reasonably reproducible task timings, an assumption that does not hold in the case of network saturation or the inability of the network to cope with a large amount of random data traffic inevitably arising with dynamic load balancing.

Figure 3 displays various performance characteristics of the COLUMBUS MR-CI code as a function of the number of CPUs. Whereas the specific numbers are problem- and machine-specific, a general pattern and conclusions are universally valid. The total transfer volume (Figure 3a) shows a minimum reflecting a good balance between memory consumption and load balancing, termed optimum work point (n_{wp}). For $n_{cpu} \ll n_{wp}$, the task size is limited by local memory shortage, and the transfer volume increases exponentially with decreasing n_{cpu}. In contrast, for $n_{cpu} \gg n_{wp}$, load balancing issues reduce the maximum task size, and the transfer volume grows monotonically. For a sufficiently large number of tasks, the task size distribution becomes inherently unfavorable as very many tiny tasks are generated, and the communication overhead can exceed the work load here. Defining "supertasks" composed of several independent small tasks sharing a common segment implements a simple semistatic load balancing which drastically reduces the transfer volume while retaining the good load balance. A number of four times n_{cpu} tasks are sufficient to ensure excellent performance (Figure 3c). A more critical quantity is the average data transfer rate per CPU, that is, the total data volume divided by the total amount of consumed CPU time per CI iteration. Here, we find typical values between 5 and 10 MB/s for semistatic and about twice this rate for dynamic load balancing. This transfer rate grows only at $\mathcal{O}(n_{cpu})^{1/3}$. Finally, we note that the communication overhead is acceptable, with almost uniformly 5−10% throughout (Figure 3d), so that the overall scaling is almost ideal.

The actual CPU time consumption and the achievable fraction of the peak performance largely depend on the use of linear algebra routines. Since it is primarily efficient cache usage that determines performance, the key feature is a large number of floating point operations per data item. BLAS levels 0 (scalar) and 1 (vector) have a ratio of 1/2, level 2 (matrix times vector) has a ratio of 1, and level 3 (matrix times matrix) has a ratio of n, where n denotes the matrix dimension. Hence, level 3 and, to some extent, level 2 operations with large n yield a significant performance boost. The evaluation of the σ vector involves a huge number of level 2 and 3 operations, where the matrix dimension is given by the number of external orbitals per irrep. A task type resolved breakdown of CPU time consumption, coupling coefficient overhead, BLAS level, and MFLOP rate is collected in Table 1. Despite the size of the eigenvalue problem of more then 1.7 billion CSFs, the individual matrix dimensions and vector lengths, respectively, amount on average to only 35 (i.e., 280 external orbitals divided by 8 irreps). Increasing the basis set size or reducing symmetry will therefore boost the efficiency. A MR-CIS calculation with the same reference configuration space solely evaluates contributions from task types $T^0_{ZZ'}$, $T^0_{YY'}$, $T^1_{YZ'}$, $T^2_{YY'}$, and T^4_{Y} at only 9% of the computational cost of the MR-CISD counterpart, while computational efficiency is fairly low due to at most matrix−vector operations and a high overhead from (scalar) coupling coefficient evaluation.

4. Results and Discussion

4.1. Computational Details. The active space consists of 12 orbitals derived from the 3d and 4s atomic orbitals. The

TABLE 1: Breakdown of the Total CPU Time Consumption for a Single Davidson Iteration for Cr_2[a]

task classes	$T^I_{ss'}$ [CPUs]	t_b %[b]	MFLOPs[c]	BLAS level[d]	n_c [10^6]
$T^0_{ZZ'}$	540	47	>35	0	173
$T^0_{YY'}$	2118	35	155	1	822
$T^0_{WW'}$, T^{0x}_{XX}	7020	3	375	1[e]	154
T^1_{YZ}	2397	41	133	1	576
T^1_{YX}, T^{1x}_{YW}	34675	4	306	2	1357
$T^2_{YY'}$	11724	2	853	2	297
T^2_{XZ}, T^{2x}_{WZ}	1077	2	560	1	8
$T^2_{XX'}$, T^2_{WX}, $T^2_{WW'}$	52801	<1	2340	3	102
T^3_{YX}, T^3_{YW}	48034	<1	770	2	5
T^4_Y, T^4_X, T^4_W	20855	0	810	2	−
sum	181241	2			3494

[a] Conditions: 1.713×10^9 CSFs, EXTD basis, 280 ext. orbitals, IBM Power4 p575, 1.6 GHz, 6.4 GFLOPs, average vector length and matrix dimension, respectively; $n = 35$. [b] Percentage of $T^I_{ss'}$ due to coupling coefficient evaluation. [c] Summed over all tasks of the given task type. [d] Terms: 0 = scalar, 1 = vector, 2 = matrix-vector, and 3 = matrix−matrix operations. [e] Vector length n^2.

MCSCF and identically the MR-AQCC reference configuration space were chosen as the direct product space of six bonding/antibonding orbital pairs occupied by two electrons each

$$(3d_{\delta_g}3d_{\delta_u})^2(3d_{\delta_g},3d_{\delta_u})^2(3d_{\pi_u}3d_{\pi_g})^2(3d_{\pi'_u}3d_{\pi'_g})^2 \times (3d_{\sigma_g},3d_{\sigma_u})^2(4s_{\sigma_g},4s_{\sigma_u})^2 \quad (21)$$

with all possible spin-couplings allowed. After reduction of the symmetry to the highest Abelian subgroup D_{2h}, a compact reference configuration space (1516 CSFs) results, as compared to the minimum CAS(12,12) with 28784 CSFs, which is still a factor of 2 smaller than the second widely used choice with 3088 CSFs.

$$(3d_{\delta_g}3d_{\delta_u})^2(3d_{\delta_g},3d_{\delta_u})^2(3d_{\pi_u}3d_{\pi_g})^2(3d_{\pi'_u}3d_{\pi'_g})^2 \times (3d_{\sigma_g},3d_{\sigma_u},4s_{\sigma_g},4s_{\sigma_u})^4 \quad (22)$$

Although both $3d_{\sigma_g}$,$4s_{\sigma_g}$ and $3d_{\sigma_u}$,$4s_{\sigma_u}$ belong pairwise to the same irrep in D_{2h}, the implicit constraint through the particular choice of the configuration space ensures the proper resolution of the active orbitals into bonding/antibonding orbital pairs. This is a crucial point for a compact wave function expansion. It is the minimum reference configuration space allowing for the correct dissociation into the pair of antiferromagnetically coupled ^7S Cr atoms.

The DKH Hamiltonian is used throughout to treat electron correlation and scalar relativistic effects on the same footing.

The extended relativistic ANO-RCC basis sets[55] are optimized for use with the DKH Hamiltonian and are sufficiently flexible to account for semicore (3s,3p) electron correlation. The TZP ([6s4p3d2f1g]), QZP ([7s5p4d3f2g1h]), and EXTD ([10s10p8d6f4g]) contractions of the primitive basis composed of (21s15p10d6f4g2h) have been used to compute between 14 and 20 points of the potential energy function. Only the spherical components of d and higher angular momentum basis functions are retained. If not otherwise stated, the chromium core ($1s^22s^22p^63s^2$) was kept frozen. Additional calculations close to r_e explore the effect of 3s electron correlation and basis set incompleteness.

The basis set superposition error (BSSE) was corrected for by the full counterpoise correction.[56] The energy of the dissociated molecule was computed in the supermolecule approach to account for size-extensivity errors.

The MR-AQCC calculations were fully uncontracted, and for the majority of the calculations, the dimension of the eigenvalue problem ranged from 163 to 1712 million CSFs, with turnaround times of about 5−10 min per CI iteration using between 32 and 512 processors of a 32-way IBM SP4 SMP cluster. The biggest calculation encountered here consisted of 2823 million CSFs with 386 basis functions. Generalized interacting space restrictions were applied.

The complete basis set (CBS) limit was estimated by two extrapolation schemes for the dynamical electron correlation energy (defined as the difference between MCSCF and MR-AQCC energies). Scheme (i) is a two-point extrapolation formula[57] widely used for the correlation-consistent (cc) basis sets by Dunning[58] applied to the TZP/QZP pair of basis sets, and scheme (ii) is the alternative scheme of approaching the CBS limit by adding successively higher angular momentum functions.[24] The contractions used are approximately radially saturated up to f and g functions ([10s10p8d6f] and [10s10p8d6f4g], respectively), and the extrapolation assumes a l^{-3} dependence of the dynamical electron correlation energy with respect to the maximum angular momentum l of the basis functions.

Spectroscopic constants were evaluated by solving the nuclear Schrödinger equation numerically using the VIBROT program from the MOLCAS[59] package as far as a sufficiently large portion of the potential energy function was available, and otherwise, they were solved by a least-squares fit to the harmonic approximation in the vicinity of the equilibrium bond length was used.

The MCSCF, MR-CISD, and MR-AQCC calculations were computed with the COLUMBUS[42] suite of quantum chemistry codes, while the integrals were obtained with the MOLCAS quantum chemistry package. Recently, we interfaced both codes (COLUMBUS-MOLCAS link) at the level of integrals, molecular orbital coefficients (energies, properties), and effective density and fock matrices (gradients), so that both single-point calculations and structure optimizations could be carried out with the combination of these codes.

4.2. The $X^1\Sigma_g^+$ State of Cr_2. The multireference character of the $X^1\Sigma_g^+$ state even close to the equilibrium bond length excludes the use of any single-reference methods. Owing to the more diffuse character of the 4s as compared to the 3d orbitals at internuclear distances of about 1.7 Å, 3d−3d bonding dominates, while toward longer bond distances, the 3d−3d bond is progressively broken, and weak 4s−4s bonding pertains at 2.5 Å. To describe bond polarization at short distances, at least f, or better g, functions are required. Due to the spatial proximity of 3d, 3p, and 3s orbitals, semicore valence polarization and electron correlation are important. The MCSCF calculations used here cannot even qualitatively account for the shape of the potential energy function but merely serve the purpose to provide qualitatively correct molecular orbitals that are resolved into pairwise bonding and antibonding orbitals. Hence, large differential dynamic electron correlation effects must be accounted for. At long bond distances, the ground state is approximately characterized by weak 4s−4s bonding and an antiferromagnetically coupled pair of $3d^5(^6S)$ cores. The basis set requirements in terms of angular momentum are much reduced, although semicore electron correlation remains significant.

The upper panel of Figure 1 displays the MR-AQCC potential computed with TZP, QZP, and EXTD basis sets along with its

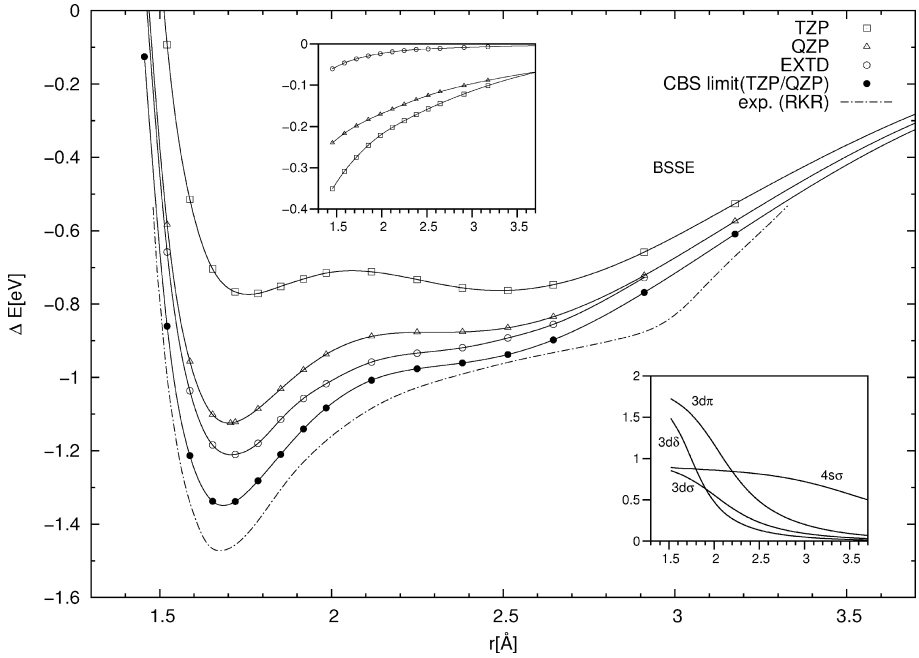

Figure 4. Computed potential energy function for Cr_2 (this work) and comparison with a potential derived from a RKR fit to experimental data. All energies are given relative to the total energy of the separated atoms in their ground state (RKR: $D_e = 1.472$ eV). Top inset: Basis set superposition error (BSSE) for TZP, QZP, and EXTD basis sets. Bottom inset: effective bond order (EBO) analysis for $3d_\sigma$, $3d_\pi$, $3d_\delta$, and $4s_\sigma$ derived from the eigenvalues of the MR-AQCC one-electron density (QZP basis).

experimental counterpart correlating the 3p, 3d, and 4s electrons. Also, the CBS limit based on the two-point extrapolation formula derived from the TZP and QZP results is displayed. All energies are given relative to the total energy of the separated atoms in their ground state. The top inset documents the internuclear distance dependence of the BSSE; while extended basis sets reasonably are saturated up to g functions (EXTD), even more, those augmented by additional h functions display a negligible BSSE of less than 0.05 eV at r_e (cf. also refs 31 and 24). Frequently used "large" QZP-like basis sets for electron correlation methods applied to first-row transition-metal compounds introduce a sizable BSSE that may not be as favorable as that in the case of ^{7}S Cr and might not be ignored from the outset.

With the TZP basis set, two distinct shallow minima at $R =$ 1.7 and 2.5 Å with almost the same energy (−0.078 eV) separated by a low barrier (barrier height 0.05 eV) are resolved. At the QZP level, the 3d−3d minimum deepens by ∼0.4 eV, while the 4s−4s bonding region is less affected. The initial barrier separating the two distinct bonding situations disappears as the 3d−3d minimum widens, owing to more flexibility to incorporate semicore valence electron correlation. The importance of single and double excitations out of the 3p semicore orbitals into the 3d/4s valence orbitals rapidly decreases with increasing bond distance. Beyond 2.25 Å, there are no core−valence excitations with a weight (c_i^2) of more than 10^{-4} contained in the wave function.

The EXTD basis yields a rather uniform reduction of the energy by 0.05 eV. After extrapolation to the CBS limit, the potential energy function closely resembles the shape of the experimental data, albeit shifted by about 0.15 eV to higher energies. The energy difference between EXTD and CBS results agrees with the corresponding energy difference for the CBS extrapolations of CIPT2 dissociation energies cross-checked against basis sets saturated up to i functions.[24] Thus, CBS limit extrapolations from TZP/QZP type contractions of ANO-RCC basis sets appear to be useful and cost-effective. However, since the TZP contraction is slightly deficient in the recoupling region between 3d−3d and 4s−4s bonding, this also slightly affects the extrapolated data in this region.

The bottom inset of Figure 4 depicts the EBO (i.e., half of the occupation number difference between bonding and antibonding natural orbitals derived from the MR-AQCC one-electron density). The total EBO drops from 4.25 at 1.72 Å to 1.44 at 2.65 Å, corresponding to breaking three bonds out of four at r_e. The δ and π bonds contribute most to bonding at r_e. While all 3d contributions vanish rapidly beyond 2.1 Å, $4s_\sigma$ though weak extends to large internuclear distances. From the data presented so far, it can be concluded (i) that MR-AQCC is capable of treating the $X^1\Sigma_g^+$ state quantitatively, provided h and i functions are incorporated, and (ii) that the shape of the experimental potential energy function is in agreement with the calculations, with the exception of the strong bend at about 2.9 Å. The reliability of the RKR potential in this region has already been questioned before.[23]

In Figure 5, current CBS extrapolated data are compared to a selection of recent work using MR-ACPF and various MRPT implementations with extended basis sets. The potential derived from CASPT2 (CAS(12,16), ANO-RCC [9s8p7d5f3g], level shift = 8.16 eV.) by Roos[23] is omitted from the plot as the resolution of the figures was insufficient. However, according to the data provided in ref 23, the shapes of the CASPT2 and the RKR potentials likely agree almost quantitatively, while $D_0 = 1.647$ eV somewhat exceeds the experimental value (cf. Table 2). In a CASPT2 calculation with a basis set close to the CBS limit (CAS(12,12), level shift = 16.33 eV),[24] D_e is overestimated by 0.35 eV. The authors pointed out that D_e depends almost linearly on the level shift beyond 10.9 eV, so that with the level shift used in ref 23, their dissociation energy should increase to in excess of 2 eV. CIPT2+Q_2, which treats solely the excitations from the core electrons perturbatively and adds a Davidson-type size-extensivity correction for the variationally treated valence electrons, is less affected by intruder states as CASPT2, though not exactly size-extensive (SCE error: 0.042

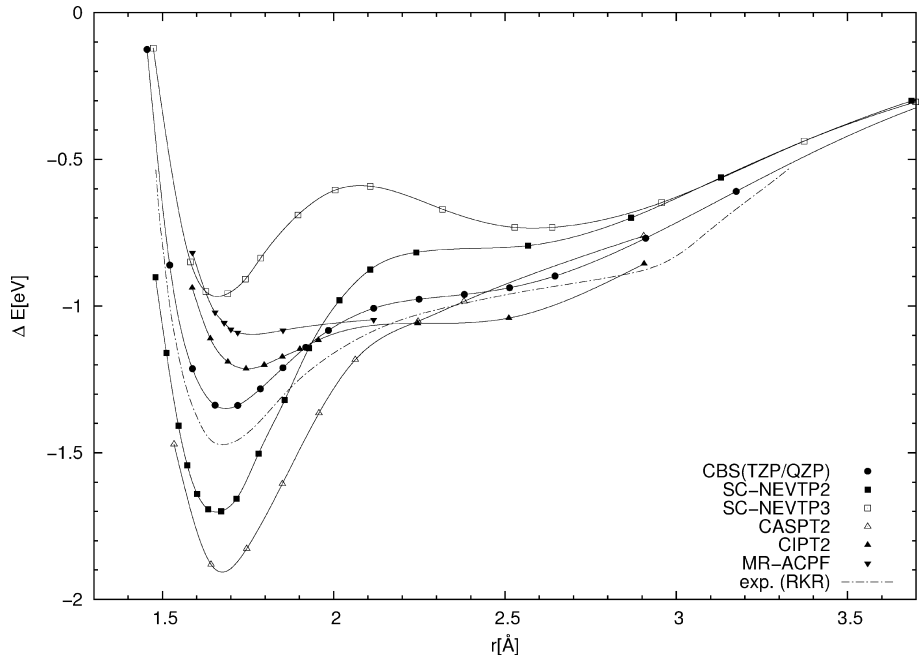

Figure 5. Potential energy function for Cr_2. All energies are given relative to the total energy of the separated atoms in their ground state (RKR: $D_e = 1.472$ eV). CBS (TZP/QZP) extrapolation of MR-AQCC data (this work), MR-ACPF (basis contains up to f functions; no scalar relativistic effects considered),[62] CIPT2 (basis includes up to i functions),[24] CASPT2 (CAS(12,12); basis includes up to i functions),[24] SC-NEVPT2 and SC-NEVPT3 (ANO-RCC basis up to h functions),[31] and experimental RKR potential.[9]

TABLE 2: Spectroscopic Constants for the $X^1\Sigma_g^+$ State of Cr_2 at the MR-AQCC Level[a]

method	basis	r_e [Å]	D_e [eV]	D_0 [eV]	ω_e [cm^{-1}]	$\Delta G_{1/2}$ [cm^{-1}]
			This Work			
MR-AQCC	TZP	1.758	0.742	−[g]	−[g]	204
MR-AQCC[b]	TZP	1.741	0.820	−	−	−
MR-AQCC	QZP	1.701	1.129	1.104	450	380
MR-AQCC[b]	QZP	1.683	1.165	−	−	−
MR-AQCC	EXTD	1.708	1.222	1.200	379	376
MR-AQCC	CBS(TZP/QZP)	1.685	1.355	1.327	459	431
MR-AQCC[b]	CBS(TZP/QZP)	1.675	1.400	−	−	−
			Other Work			
MR-ACPF[c]	f	1.72	1.09	1.05	339	−
IC-MRCI+Q_2[d]	fgh	1.666	1.10	1.07	512	−
CIPT2+Q_2[d]	fgh	1.753	1.21	1.19	321	
CIPT2+Q_2[b,d]	fgh	1.756	1.20	1.18	322	−
CASPT2(g_1)[d]	fgh	1.674	1.88	1.85	571	−
CASPT2(g_1)[b,d]	fgh	1.678	1.87	1.84	565	−
CASPT2(g_1)[b,e]	ANO-RCC fg	1.662	−	1.647	−	413
SC-NEVPT2[f]	ANO-RCC fgh	1.655	−	1.702	−	580
SC-NEVPT3[f]	ANO-RCCfgh	1.671	−	0.966	−	491
experiment		1.679[h]	1.472 ± 0.056[i]	1.443 ± 0.056[j]	481[m]	452[h]
			1.56 ± 0.06[i]	1.53 ± 0.06[k]		
			1.45 ± 0.1[i]	1.42 ± 0.1[l]		

[a] The 3p,3d,4s electrons correlated. [b] Including 3s electron correlation. [c] Reference 62. [d] Reference 24. [e] Reference 23. [f] Reference 31. [g] Harmonic approximation inappropriate for shallow double minimum. [h] Reference 1. [i] Vibrational zero-point energy of 0.029 eV assumed. [j] Reference 2. [k] Reference 61. [l] Reference 60. [m] Reference 9.

eV).[24] It shows the opposite behavior and underestimates D_e by 0.25 eV. Additionally, these authors point out that both CASPT2 and, to a lesser extent, CIPT2+Q_2 fail to describe core and valence electron correlation properly balanced,[24] that is, the inclusion of 3p electron correlation leads to an increase of r_e.

MR-CI+Q and equally MR-AQCC, however, produce the expected result that 3p electron correlation reduces r_e. For MR-AQCC (QZP contraction), a linear relation between r and the 3p core correlation energy (in atomic units) in the vicinity of the experimental equilibrium bond length was found ($-0.587 + 0.016(r - 3.0)$). The 3s electron correlation is, not unexpectedly, rather indifferent to the chemical bond ($-0.1778 + 0.002(r - 3.0)$). Since CASPT2 yields an excellent equilibrium bond length and harmonic frequency, error compensation between valence and core electron correlation must play a role. NEVPT2 and NEVPT3 by construction do not encounter intruder state problems. While NEVPT2 also overestimates D_e by 0.25 eV, NEVPT3 produces a potential energy function with two pronounced minima separated by a barrier of ~0.3 eV, vaguely similar to the MR-AQCC data computed with the TZP basis set. Note that while CASPT2, CIPT2+Q_2, MR-ACPF, and MR-AQCC describe the 4s−4s bonding region in agreement with

TABLE 3: Size-Consistency Error of Cr_2 in eV Evaluated at an Interatomic Separation of 16 Å (EXTD basis set)

	correlated electrons		
method	3d4s	3p3d4s	3s3p3d4s
MR-CISD	0.185	1.047	1.369
MR-CISD+Q_1	0.054	0.401	0.542
MR-CISD+Q_2	0.040	0.287	0.385
MR-CISD+Q_3	0.024	0.141	0.179
MR-ACPF	0.000	0.000	0.000
MR-AQCC	0.008	0.013	0.012

experimental data, both NEVPT2 and NEVPT3 curves are too shallow.

There is some controversy in the literature about the presence of a second (shallow) minimum in the 4s−4s bonding region. While experimental data are insufficient to unequivocally assign a second minimum, CIPT2 seems to predict at most a very shallow minimum at about $r = 2.4$ Å, while MR-AQCC with large basis sets indicates an almost flat shelf extending over 0.25 Å at about $r = 2.4$ Å. The double minimum observed for the TZP basis is an artifact of an insufficiently flexible basis set. CASPT2 calculations also do not indicate a double minimum.

Considering the discussion about the shortcomings of the perturbation-theory-based approaches, it seems likely that the choice of the zeroth-order Hamiltonian is the primary source of error. For CASPT2 additionally, the level shift procedure is another likely source of error. While the discussed multireference approaches have been shown to work very well for a wide range of applications, one has to accept that especially for the ground state of the chromium dimer, it is difficult to obtain a good zeroth-order Hamiltonian as the size of the active space is quite limited. Given the results, the CAS(12,16) reference space appears to be a step toward the right direction. However, the basis set used there is considerably smaller than many of those discussed so far, and the correction to the CBS limit may be sizable.

The spectroscopic constants are collected in Table 2. The equilibrium bond length from MR-AQCC with the EXTD basis is too long by 0.03 Å. Extrapolation to the CBS limit and 3s electron correlation reduce r_e to about the experimental value. Extrapolated D_e underestimates the experimental value still by about 0.1 eV, while ω_e is about right. The energies of the higher vibrational states obtained by solving the nuclear Schrödinger equation numerically with the TZP/QZP extrapolated potential (not given here) are somewhat low.

In Table 3, the size-consistency error (SCE) for the $X^1\Sigma_g^+$ state evaluated at an internuclear distance of 16 Å is collected for MR-CISD, MR-CISD with several variants of the Davidson correction, MR-ACPF, and MR-AQCC correlating different numbers of electrons. The SCE of straightforward MR-CISD is unacceptable for 18 and more correlated electrons. The Q_3 variant of the Davidson correction works throughout best and reduces the SCE by 87% as compared to MR-CISD. MR-AQCC reduces the SCE by 99%, and MR-ACPF is practically free of SCE. We have already briefly discussed that intruder states can occur in the MR-AQCC method. In the case of the ground state of Cr_2, there is no indication for the presence of an intruder state; the weight of the reference wave function (c_0^2) within the bonding regime varies between 0.82 and 0.84, no single nonreference CSF gains a remarkable weight, and the second excited singlet state of Σ_g^+ symmetry is well-separated by more than 2.5 eV and dissociates to a pair of ^5S chromium atoms.

Finally, basis set effects on the dissociation energy evaluated at 1.7075 Å using various contractions of the ANO-RCC basis set are shown in Table 4. The 3s electrons have been kept frozen here. A cc-like contraction sequence of the ANO-RCC basis set ([6s4p3d2f1g] $X = 3$, [7s5p4d3f2g1h] $X = 4$, CBS limit thereof) seems to be somewhat low. Comparison with scheme (ii) using the contractions [10s10p8d6f] and [10s10p8d6f4g] yields a CBS limit of 1.45 eV. Inspecting the effect of an h functions in comparison with the effect of a single set of i functions suggests that the h function exponents are not optimum. Hence, the CBS(TZP/QZP) extrapolation underestimates the actual CBS limit by 0.09−0.12 eV. Adding the 3s electron correlation contribution of 0.06 eV, a final D_e of 1.48−1.50 eV would be expected. Given the comparatively small basis set of the CASPT2 calculation with the enlarged active space,[23] the corresponding CBS limit for D_e may be expected at about 1.88 eV.

TABLE 4: Basis Set Effects on D_e Evaluated at the MR-AQCC Level of Theory with 3s Semicore Electrons Frozen at 1.7075 Å Using the ANO-RCC Basis Set[a]

contraction	D_e [eV]	E(MR-AQCC)+ 2100[b] [E_h]	#CSF [10^6]
[6s4p3d2f1g]	0.76	−0.06166	163
[7s5p4d3f2g]	1.09	−0.12602	406
[7s5p4d3f2g1h]	1.12	−0.14626	547
[7s5p4d3f2g1h][c]	1.18	−0.32739	741
[10s10p8d6f]	0.92	−0.08530	1043
[10s10p8d6f4g]	1.21	−0.16213	1713
[10s10p8d6f4g2h]	1.30	−0.18589	2290
[10s10p8d6f4g2h1i]	1.42	−0.19124	2826
CBS([6s4p3d2f1g]/[7s5p4d3f2g1h])[d]	1.33		
CBS([10s10p8d6f]/[10s10p8d6f4g])[e]	1.45		

[a] Basis set exponents for the h and i functions are 2.543, 0.943 (h), and 1.10 (i). [b] Total energy in atomic units excluding BSSE corrections. [c] The 3s electrons correlated. [d] Scheme (i). [e] Scheme (ii).

5. Summary and Conclusions

The potential energy function of the Cr_2 $X^1\Sigma_g^+$ has been investigated with the multireference-averaged quadratic coupled cluster (MR-AQCC) method. Large fully uncontracted MR-AQCC calculations with large basis sets resulted in huge wave function expansions of up to 2.8 billion CSFs, requiring an efficient parallel implementation of the code. Relevant implementation details have been described, and the general performance characteristics of the implementation have been discussed.

It has been demonstrated that MR-AQCC is a method applicable to the accurate calculation of the $X^1\Sigma_g^+$ of the chromium dimer. Basis set studies including 3p electron correlation have been used to extrapolate the entire potential energy function to the estimated complete basis set limit. The quality of the extrapolation scheme has been assessed by additional calculations with even larger basis sets up to including i functions. While the computed $r_e = 1.675$ Å and $\omega_e = 459$ cm^{-1} agree well with the experimental data ($r_e = 1.679$ Å, $\omega_e = 481$ cm^{-1}), the energy of higher vibrational states differs somewhat, and D_e is underestimated by ∼0.13 eV. Further, MR-AQCC calculations with large basis set and consideration of 3s correlation effects in the vicinity of the equilibrium bond length indicate that 0.1 eV is due to deficiencies of the TZP/QZP-based CBS extrapolation and that 0.06 eV arises from 3s electron correlation.

On the basis of the MR-AQCC results and comparison with recent data from the literature, we arrive at the conclusion that multireference perturbation theory has substantial difficulties in treating the chromium dimer ground state, owing to an inadequate zeroth-order approximation and due to intruder state

problems (where applicable). While at second-order perturbation theory these deficiencies have only moderate impact so that the overall agreement with experimental data is quite good, the notion that the agreement primarily arises from error compensation effects is worrysome. Third-order perturbation theory produced poor results, and in light of the presented data, they are likely artifacts from the choice of the zeroth-order Hamiltonian. CASPT2 data with an extended CAS(12,16), which are in good agreement with experimental data, are an indication of stricter requirements on the choice of $\hat{H}_0$ while MR-AQCC does not share this sensitivity toward the reference space.

Acknowledgment. The calculations have been carried out on the supercomputer resources provided by the John-von-Neumann Institute for Computing (NIC) at the Research Centre, Jülich. A generous supply of computing time is gratefully acknowledged. This work has been partially supported by the European Community (COST Action D37).

References and Notes

(1) Bondybey, V. E.; English, J. H. *Chem. Phys. Lett.* **1983**, *94*, 443.
(2) Hilpert, K.; Ruthard, K. *Ber. Bunsen-Ges. Phys. Chem.* **1987**, *91*, 724.
(3) Rohlfing, E. A.; Valentini, J. J. *J. Chem. Phys.* **1986**, *84*, 6560.
(4) Roos, B. O.; Borin, A. C.; Gagliardi, L. *Angew. Chem., Int. Ed.* **2007**, *46*, 1469.
(5) Roos, B. O.; Malmqvist, P.-A.; Gagliardi, L. *J. Am. Chem. Soc.* **2006**, *128*, 17000.
(6) Borin, A. C.; Gobbo, J. P.; Roos, B. O. *Chem. Phys.* **2008**, *343*, 210.
(7) Andersson, K.; Roos, B. O. In *Modern electron structure theory*; Yarkony, R., Ed.; World Scientific: Singapore, 1995; Vol. 2, p , I:55.
(8) Roos, B. O.; Andersson, K.; Fülscher, M.; Malmqvist, P.-A.; Serrano-Andres, L.; Pierloot, K.; Merchan, M. In *Multiconfigurational perturbation theory: Applications in electronic spectroscopy*; Prigogine, I., Rice, S. A., Eds.; John Wiley & Sons Ltd.: New York, 1996; Vol. 93, p 219.
(9) Casey, S. M.; Leopold, D. G. *J. Phys. Chem.* **1993**, *97*, 816.
(10) Bauschlicher, C. W., Jr.; Patridge, H. *Chem. Phys. Lett.* **1994**, *231*, 277.
(11) Thomas, E. J., III; Murray, J. S.; O'Connor, C. J.; Politzer, P. *J. Mol. Struct.* **1999**, *487*, 177.
(12) Desmerais, N.; Reuse, F. A.; Khanna, S. N. *J. Chem. Phys.* **2000**, *112*, 5576.
(13) Salahub, D. R. In *Ab Initio Methods in Quantum Chemistry*; Lawley, K. P., Ed.; John Wiley & Sons Ltd.: Chichester, England, 1987; Vol. 69, p 447.
(14) Dunlap, B. I. *Phys. Rev. A* **1983**, *27*, 2217.
(15) Delley, B.; Freeman, A. J.; Ellis, D. E. *Phys. Rev. Lett.* **1983**, *50*, 488.
(16) Baykara, N. A.; McMaster, B. N.; Salahub, D. R. *Mol. Phys.* **1984**, *52*, 891.
(17) Becke, A. D. *J. Chem. Phys.* **1986**, *84*, 4524.
(18) Edgecombe, K. E.; Becke, A. D. *Chem. Phys. Lett.* **1995**, *244*, 427.
(19) Cheng, H.; Wang, L. S. *Phys. Rev. Lett.* **1996**, *77*, 51.
(20) Brynda, M.; Gagliardi, L.; Roos, B. O. *Chem. Phys. Lett.* **2009**, *471*, 1.
(21) Roos, B. O. In *Ab Initio Methods in Quantum Chemistry*; Lawley, K. P., Ed.; John Wiley & Sons Ltd.: Chichester, England, 1987; Vol. 69, p 399.
(22) Roos, B. O. *Acc. Chem. Res.* **1999**, *32*, 137.
(23) Roos, B. O. *Collect. Czech. Chem. Commun.* **2003**, *68*, 265.
(24) Celani, P.; Stoll, H.; Werner, H.-J.; Knowles, P. J. *Mol. Phys.* **2004**, *102*, 2369.
(25) Angeli, C.; Cimiraglia, R.; Evangelisti, S.; Leininger, T.; Malrieu, J.-P. *J. Chem. Phys.* **2001**, *114*, 10252.
(26) Angeli, C.; Cimiraglia, R.; Malrieu, J.-P. *Chem. Phys. Lett.* **2001**, *350*, 297.
(27) Angeli, C.; Cimiraglia, R.; Malrieu, J.-P. *J. Chem. Phys.* **2002**, *117*, 9138.
(28) Angeli, C.; Borini, S.; Cestari, M.; Cimiraglia, R. *J. Chem. Phys.* **2004**, *121*, 4043.
(29) Roos, B. O.; Andersson, K. *Chem. Phys. Lett.* **1995**, *245*, 215.
(30) Forsberg, N.; Malmquist, P. A. *Chem. Phys. Lett.* **1997**, *274*, 196.
(31) Angeli, C.; Bories, B.; Cavallini, A.; Cimiraglia, R. *J. Chem. Phys.* **2006**, *124*, 054108.
(32) Werner, H.-J.; Knowles, P. J. *Theor. Chim. Acta* **1990**, *78*, 175.
(33) Davidson, E. R.; Silver, D. W. *Chem. Phys. Lett.* **1977**, *52*, 403.
(34) Szalay, P. G.; Bartlett, R. J. *J. Chem. Phys.* **1995**, *103*, 3600.
(35) Szalay, P. G.; Bartlett, R. J. *Chem. Phys. Lett.* **1993**, *214*, 481.
(36) Hess, B. A. *Phys. Rev.* **1986**, *A33*, 3742.
(37) Hess, B. A.; Jansen, G. *Phys. Rev.* **1989**, *A39*, 6016.
(38) Dachsel, H.; Lischka, H.; Shepard, R.; Nieplocha, J.; Harrison, R. J. *J. Comput. Chem.* **1997**, *18*, 430.
(39) Lischka, H.; Shepard, R.; Brown, F. B.; Shavitt, I. *Int. J. Quantum Chem.* **1981**, *S15*, 91.
(40) Shepard, R.; Shavitt, I.; Pitzer, R. M.; Comeau, D. C.; Pepper, M.; Lischka, H.; Szalay, P. G.; Ahlrichs, R.; Brown, F. B.; Zhao, J. *Int. J. Quantum Chem.* **1988**, *S22*, 149.
(41) Lischka, H.; Shepard, R.; Pitzer, R. M.; Shavitt, I.; Dallos, M.; Müller, T.; Szalay, P. G.; Seth, M.; Kedziora, G. S.; Yabushita, S.; Zhang, Z. *Phys. Chem. Chem. Phys.* **2001**, *3*, 664.
(42) Lischka, H.; Shepard, R.; Shavitt, I.; Pitzer, R. M.; Dallos, M.; Müller, T.; Szalay, P. G.; Brown, F. B.; Ahlrichs, R.; Boehm, H. J.; Chang, A.; Comeau, D. C.; Gdanitz, R.; Dachsel, H.; Ehrhardt, C.; Ernzerhof, M.; Höchtl, P.; Irle, S.; Kedziora, G.; Kovar, T.; Parasuk, V.; Pepper, M. J. M.; Scharf, P.; Schiffer, H.; Schindler, M.; Schüler, M.; Seth, M.; Stahlberg, E. A.; Zhao, J.-G.; Yabushita, S.; Zhang, Z.; Barbatti, M.; Matsika, S.; Schuurmann, M.; Yarkony, D. R.; Brozell, S. R.; Beck, E. V.; Blaudeau, J.-P. COLUMBUS, an ab-initio electronic structure program, release 5.9.2.JSC 2008, www.univie.ac.at/columbus.
(43) Gdanitz, R. J.; Ahlrichs, R. *Chem. Phys. Lett.* **1988**, *143*, 413–413.
(44) Szalay, P. G.; Müller, T.; Lischka, H. *Chem. Phys. Phys. Chem.* **2000**, *2*, 2067.
(45) Szalay, P. G. *Chem. Phys.* **2008**, *349*, 121.
(46) Shepard, R. In *Modern Electronic Structure Theory*; Yarkony, D. R., Ed.; Advanced Series in Physical Chemistry; World Scientific: Singapore, 1995; p 345.
(47) Shepard, R.; Kedziora, G. S.; Lischka, H.; Shavitt, I.; Mueller, T.; Szalay, P. G.; Kallay, M.; Seth, M. *Chem. Phys.* **2008**, *349*, 37.
(48) Shavitt, I. In *The Unitary Group for the Evaluation of Electronic Energy Matrix Elements*; Hinze, P., Ed.; Lecture Notes in Chemistry; Springer: Berlin, Germany, 1981; p 51.
(49) Shavitt, I. In *Mathematical Frontiers in computational Chemical Physics*; Truhlar, D. G., Ed.; Springer: New York, 1988; p 300.
(50) Shepard, R.; Minkoff, M. *Int. J. Quantum Chem.* **2006**, *106*, 3190.
(51) Roos, B. O.; Siegbahn, P. E. M. In *The Direct Configuration Interaction Method from Molecular Integrals*; Schaefer, H. F., III, Ed.; Methods of Electronic Structure Theory; Plenum Press: New York, 1977; p 345.
(52) Davidson, E. R. *J. Comput. Phys.* **1975**, *17*, 87.
(53) Davidson, E. R. *Comput. Phys.* **1993**, *7*, 519.
(54) Shepard, R.; Shavitt, I.; Lischka, H. *J. Comput. Chem.* **2002**, *23*, 1121.
(55) Roos, B. O.; Lindh, R.; Malmqvist, P.-A.; Veryazov, V.; Widmark, P.-O. *J. Chem. Phys. A* **2005**, *109*, 6575.
(56) Boys, S. F.; Bernardi, F. *Mol. Phys.* **1970**, *19*, 553.
(57) Bak, K. L.; Gauss, J.; Jørgensen, P.; Olsen, J.; Helgaker, T.; Stanton, J. F. *J. Chem. Phys.* **2001**, *114*, 6548.
(58) Dunning, T. H. *J. Chem. Phys.* **1989**, *90*, 1007.
(59) Karlstrom, G.; Lindh, R.; Malmqvist, P.-A.; Roos, B. O.; Ryde, U.; Veryazov, V.; Widmark, P.-O.; Cossi, M.; Schimmelpfennig, B.; Neogrady, P.; Seijo, L. *Comput. Mater. Sci.* **2003**, *28*, 222.
(60) Su, C.-X.; Hales, D. A.; Armentrout, P. B. *Chem. Phys. Lett.* **1993**, *201*, 199.
(61) Simard, B.; Lebeault-Dorget, M.-A.; Marijnissen, A.; ter Meulen, J. *J. Chem. Phys.* **1998**, *108*, 9668.
(62) Dachsel, H.; Harrison, R. J.; Dixon, D. A. *J. Phys. Chem. A* **1999**, *103*, 152.

JP905254U